Inorg. Chem. **2009**, *48*, 3993−4002

Structure and Dynamics of the U^{4+} Ion in Aqueous Solution: An ab Initio Quantum Mechanical Charge Field Molecular Dynamics Study

Robert J. Frick, Andreas B. Pribil, Thomas S. Hofer, Bernhard R. Randolf, Anirban Bhattacharjee, and Bernd M. Rode*

Theoretical Chemistry Division, Institute of General, Inorganic and Theoretical Chemistry, University of Innsbruck, Innrain 52a, A-6020 Innsbruck, Austria

Received August 14, 2008

The structure and dynamics of the stable four-times positively charged uranium(IV) cation in aqueous solution have been investigated by ab initio quantum mechanical charge field (QMCF) molecular dynamics (MD) simulation at the Hartree−Fock double-ζ quantum mechanical level. The QMCF-MD approach enables investigations with the accuracy of a quantum mechanics/molecular mechanics approach without the need for the construction of solute−solvent potentials. Angular distribution functions; radial distribution functions; coordination numbers of the first, second, and third shell (9, 19, and 44, respectively); coordination number distribution functions; tilt- and Θ-angle distribution functions; as well as local density corrected triangle distribution functions have been employed for the evaluation of the hydrated ion's structure. Special attention was paid to the determination of the geometry of the first hydration layer, and the results were compared to experimental large-angle X-ray scattering and extended X-ray absorption fine structure data. The solvent dynamics around the ion were also investigated using mean ligand residence times and related data and, resulting from the unavailability of any experimental data, were compared to ions with similar properties.

1. Introduction

A rising number of publications on the structure and the dynamics of different actinide ions and actinide-containing complexes have been published within the past decade, many of them outlining the importance of agglomerating profound knowledge about the microscopic properties of these species to assist all kinds of nuclear-technology-related research. An extensive review paper[1] refers to, among many analytical aspects, most of this recent work. The investigation of microscopic properties of the actinides in aqueous solution is hindered by some serious obstacles, for experimentalists as well as for theoreticians.[2] Present force fields are poorly parametrized for these species and do not allow precise insights, but even the mere amount of electrons handicaps quantum chemical treatment due to the computational demand. The increasing influence of special relativity, spin−orbit coupling, and multiplet and correlation effects with increasing atomic number also poses an obstacle. On the experimental side, they require delicate handling due to their radioactivity, and the interpretation of results is challenging due to a wide range of oxidation states and coordination numbers adopted. On the other hand, their high electron density is beneficial to both extended X-ray absorption fine structure (EXAFS) and large-angle X-ray scattering (LAXS) methods, and last but not least, the addressed wealth in structures and oxidation states poses an academically interesting field of activity to theoretical chemistry.

The U^{4+} ion is one of the very few atomic ions known to remain stable in (acidic) aqueous solution carrying a 4-fold positive charge. Due to the high charge and the neutral environment in the used simulation box, hydrolysis was expected but did not take place during the simulation time of more than 10 ps. Structural data obtained from LAXS[3−5] and EXAFS[6] experiments are available, and the closely

* To whom correspondence should be addressed. Tel.: +43-512-507-5160. Fax: +43-512-507-2714. E-mail: Bernd.M.Rode@uibk.ac.at.

(1) Szabó, Z.; Toriashi, T.; Vallet, V.; Grenthe, I. *Coord. Chem. Rev.* **2006**, *250*, 784.
(2) Pepper, M.; Bursten, B. E. *Chem. Rev.* **1991**, *91*, 719.
(3) Johansson, G. *Acta Chem. Scand.* **1968**, *22*, 399.
(4) Pocev, S.; Johannson, G. *Acta Chem. Scand.* **1973**, *27*, 2146.
(5) Johansson, G.; Magini, M.; Ohtaki, H. *J. Solution Chem.* **1991**, *20*, 775.
(6) Moll, H.; Denecke, M. A.; Jalilehvand, M. A. F.; Sandström, M.; Grenthe, I. *Inorg. Chem.* **1999**, *38*, 1795.

10.1021/ic801554p CCC: $40.75
Published on Web 04/01/2009

related Th^{4+} ion has been theoretically investigated.[7−10] Curium(III) has been studied using MD and DFT methods by Yang et al., comparing results for structure and exchange dynamics compared with experimental data.[11] Still, to our best knowledge, no comprehensive theoretical treatment of the U(IV) ion in water has been published yet, and a precise quantum chemical simulation will assist in correctly interpreting experimental data and provide more detailed knowledge about this ion in solution.

2. Methods

A conventional quantum mechanics/molecular mechanics (QM/MM) formalism[12,13] demands the construction of pair, three-body, and even higher many-body potential functions between the species inside and outside the QM region to evaluate their interactions. This is usually achieved by ab initio evaluation of single points on the energy surface and subsequent fitting of analytical functions, a very time-consuming labor. Inevitably, a strongly polarized system like the U(IV) ion and one water in the gaseous phase produces charge transfer effects that in turn lead to unphysical potentials, which dismisses the possibility of the application of such an approach to the uranium(IV) ion in water. The *quantum mechanical charge field molecular dynamics* (QMCF-MD) approach[14,15] maintains the partition between a QM region and an MM region but does not require any potential functions but the ones for solvent−solvent interactions. Therefore, QMCF constitutes an easy approach to ab initio simulations of many different solutes in water.[16−21] As far as the MM part is concerned, the BJH-CF2 water model[22,23] has been picked for its flexibility, since an intramolecular potential term allows explicit hydrogen movements. QM/MM studies of pure water[24] have confirmed the good quality of this model.

In QMCF-MD, the QM region is enlarged to an extent where it also covers the second layer of hydration and is divided into two subregions, of which the so-called core zone contains any solute of choice and the first shell of the coordinating water molecules and the so-called layer zone contains another shell of solvent molecules (Figure 1). Therefore, if the layer zone is at least 3-Å-thick, any non-Coulombic interaction between the core zone and the MM region is sufficiently small to be neglected.

$$F_J^{\text{core}} = F_J^{\text{QM}} + \sum_{I=1}^{M} \frac{q_J^{\text{QM}} \cdot q_I^{\text{MM}}}{r_{IJ}^2} \cdot \left[1 + 2 \cdot \frac{\varepsilon + 1}{2\varepsilon - 1} \cdot \left(\frac{r_{IJ}}{r_c}\right)^3\right] \quad (1)$$

$$F_J^{\text{layer}} = F_J^{\text{QM}} + \sum_{I=1}^{M} \left\{ \frac{q_J^{\text{QM}} \cdot q_I^{\text{MM}}}{r_{IJ}^2} \cdot \left[1 + 2 \cdot \frac{\varepsilon + 1}{2\varepsilon - 1} \cdot \left(\frac{r_{IJ}}{r_c}\right)^3\right] + F_{IJ}^{\text{nC}} \right\} \quad (2)$$

The force expression for a particle J in the layer zone, F_J^{layer}, adds a term for non-Coulombic interactions with the molecular mechanically treated bulk solvent. The fact that only water molecules are present in the outer QM region saves the construction of ab initio pair and three-body potentials for the solute−water interactions. Both force expressions for the QM regions use electrostatic embedding, the addition of a perturbation term $\hat{V}'$ to the core Hamiltonian $\hat{h}_{\text{HF}}{}^{c}$:

$$\hat{h}_{\text{QMCF}}^{c} = \hat{h}_{\text{HF}}^{c} + \hat{V}' \quad (3)$$

$$\hat{V}' = \sum_{J=1}^{M} \frac{q_J}{r_{iJ}} \quad (4)$$

A MM particle's force term, F_J^{MM}, employs solvent−solvent potential functions to describe the interaction with all water molecules in the layer zone as well as the bulk region. Non-Coulombic interactions with the core zone particles, again, are neglected. The Coulombic interactions are expressed as a sum of point charges, derived and updated with the aid of Mulliken population analysis[25] in every step of the simulation for all QM particles and taken from the force field point charges for all MM particles. The assignment of partial charges to atoms based on a distribution of the electron density or via fitting of charges to mimic precomputed potential surfaces has no physical meaning, as partial charges are nonobservable properties. The same is true for the charges assigned to the MM model representing the solvent

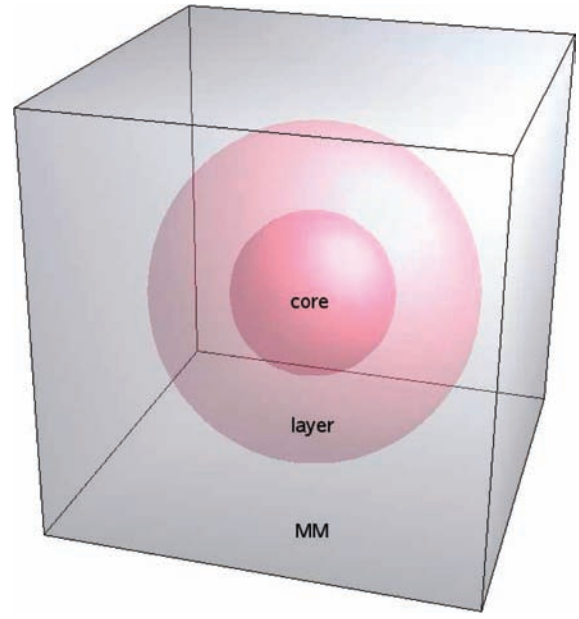

Figure 1. Schematic drawing of the simulation box partitioned into the QM core and layer region. The remaining simulation box is treated by classical molecular mechanics.

(7) Tsushima, S.; Reich, T. *Chem. Phys. Lett.* **2001**, *347*, 127.
(8) Tsushima, S. *J. Phys. Chem. B* **2008**, *112*, 7080.
(9) Yang, T.; Tsushima, S.; Suzuki, A. *Chem. Phys. Lett.* **2002**, *360*, 534.
(10) Yang, T.; Tsushima, S.; Suzuki, A. *J. Solid State. Chem.* **2003**, *171*, 235.
(11) Yang, T.; Bursten, E. B. *Inorg. Chem.* **2006**, *45*, 5291.
(12) Field, M. J.; Bash, P. A.; Karplus, M. *J. Comput. Chem.* **1990**, *11*, 700.
(13) Bakowies, D.; Thiel, W. *J. Phys. Chem.* **1996**, *100*, 10580.
(14) Rode, B. M.; Hofer, T. S.; Randolf, B. R.; Schwenk, C. F.; Xenides, D.; Vchirawongkwin, V. *Theor. Chem. Acc.* **2006**, *115*, 77.
(15) Rode, B. M.; Hofer, T. S. *Pure Appl. Chem.* **2006**, *78*, 525.
(16) Fatmi, M. Q.; Hofer, T. S.; Randolf, B. R.; Rode, B. M. *J. Comput. Chem.* **2007**, *28*, 1704.
(17) Vchirawongkwin, V.; Rode, B. M. *Chem. Phys. Lett.* **2007**, *443*, 152.
(18) Vchirawongkwin, V.; Persson, I.; Rode, B. M. *J. Phys. Chem. B* **2007**, *111*, 4150.
(19) Pribil, A. B.; Hofer, T. S.; Vchirawongkwin, V.; Randolf, B. R.; Rode, B. M. *Chem. Phys.* **2008**, *346*, 182.
(20) Pribil, A. B.; Hofer, T. S.; Randolf, B. R.; Rode, B. M. *J. Comput. Chem.* **2008**, *29*, 2330.
(21) Hofer, T. S.; Randolf, B. R.; Adnan, A. S.; Rode, B. M.; Persson, I. *Chem. Phys. Lett.* **2007**, *445*, 193.
(22) Stillinger, F. H.; Rahmann, A. *J. Chem. Phys.* **1978**, *68*, 666.
(23) Bopp, P.; Jancso, G.; Heinzinger, K. *Chem. Phys. Lett.* **1983**, *98*, 129.
(24) Xenides, D.; Randolf, B. R.; Rode, B. M. *J. Chem. Phys.* **2005**, *122*, 4506.

in the MM region. In QM/MM studies, the criterion of compatibility of QM and MM treatment is of the utmost importance and has priority over other arguments. The use of Mulliken populations for the embedding procedure in connection with BJH-CF2[22,23] has proven to be the best choice in earlier works.[18,19,54,55] As the level of theory as well as the basis set assigned to oxygen and hydrogen atoms are the same in this study, a similar performance is expected.

$$F_J^{\mathrm{MM}} = \sum_{\substack{I=1 \\ I\neq J}}^{M} F_{IJ}^{\mathrm{MM}} + \sum_{I=1}^{N_1+N_2} \frac{q_I^{\mathrm{QM}} \cdot q_J^{\mathrm{MM}}}{r_{IJ}^2} \cdot \left[1 + 2 \cdot \frac{\varepsilon + 1}{2\varepsilon - 1} \cdot \left(\frac{r_{IJ}}{r_c}\right)^3\right] + \sum_{I=1}^{N_2} F_{IJ}^{\mathrm{nC}} \quad (5)$$

The QM potential $V(r)$ at the QM to MM boundary is noncontinuous due to the different directions of the regions' force. To ensure a continuous transition, a smoothing function, $S(r)$, is used to establish an appropriate potential $V_s(r)$.

$$S(r) = \frac{(r_c^2 - r^2)^2 \cdot (r_c^2 + 2r^2 - 3(r_c + \Delta r)^2)}{(r_c^2 - (r_c + \Delta r)^2)^3} \quad (6)$$

$$V_s(r) = V(r), \quad \text{for } r < r_c \quad (7)$$

$$V_s(r) = V(r) \cdot S(r), \quad \text{for } r_c \leq r \leq r_c + \Delta r \quad (8)$$

$$V_s(r) = 0, \quad \text{for } r > r_c + \Delta r \quad (9)$$

As a result, the smoothed potential, $V_s(r)$, and its derivatives stay continuously differentiable in the region of the cutoff. The smoothing region, Δr, is chosen to be 0.2 Å by default.

Reference 14 gives further insight into the QMCF methodology.

2.1. Simulation Details. The choice of Dunning DZP basis sets for oxygen and hydrogen atoms[26,27] was based on earlier QM/MM simulation work on solvated ions.[15,28,29] In the literature[30,31] and in electronic basis set libraries,[31] several different basis sets and effective core potentials (ECPs) for the uranium atom are available: CRENBL ECP, LANL2DZ ECP, Stuttgart RLC ECP, Stuttgart RSC 1997 ECP, and ECP60MHF +ECP from Stuttgart and Küchle et al.[61] The first four were tested with different uranium(IV)−water gas-phase clusters using the Gaussian03[32] and Turbomole[33−36] software packages. Unfortunately, most of our test calculations with these atom-optimized basis sets for the U^{4+} uranium suffered from convergence problems which have not been reported for similar calculations, for example, for AnF_6 by Batista et al.[63] Gas-phase clusters of the uranyl(VI) ion with water have been calculated in the course of similar work[37] (with one water molecule coordinating to each of the oxygen atoms and five water ligands coordinating to the uranium center), and it was assumed that a basis set proven suitable for UO_2^{2+} would also be appropriate for U^{4+}. The results are shown in Table 1. The Stuttgart RSC 1997 ECP basis set[38] with a relativistically corrected ECP accounting for 60 inner electrons was chosen for reasons of satisfactory stability and results, keeping computational power at an affordable extent. The ECP of this basis set was initially constructed for application with Gaussian 03 and had to be replaced with the ECP for uranium from the Turbomole library for the QMCF molecular dynamics simulation, since the QMCF code currently has a Turbomole interface only. This exchange resulted in values for geometries and energies of the gas clusters identical to those obtained with the original Stuttgart RSC 1997 ECP.

Table 1. Average Distance in Ångstroms between the Uranium and the Water Oxygen As Well As Interaction Energies Per Ligand ΔE in kilocalories per mole for Uranyl(VI)−Water Clusters for Different Basis Sets and Methods[a]

H_2O ligands	basis set	method	dist. U−OH_2 [Å]	ΔE [kcal/mol]
1	Stuttgart RSC[38]	HF	2.35	−76.13
		B3LYP	2.32	−76.15
		MP/2	2.31	−76.27
		CCSD	2.32	−76.32
5	CRENBL[40]	HF	2.50	
		MP/2	2.49	
5	LANL2DZ	HF	2.51	
	(unpublished, used in ref 41)	MP/2	2.52	
5	Stuttgart RLC[38]	HF	2.51	
		MP/2	2.47	
5	Stuttgart RSC[38]	HF	2.52	−76.01
		B3LYP	2.48	−76.53
		MP/2	2.48	−76.15

[a] Values taken from ref 37.

Table 1 contains information about U−OH_2 bonding distances of the UO_2^{2+} clusters calculated at HF, hybrid density functional B3LYP, second-order Møller−Plesset, and CCSD levels of theory. Present computational facilities only allow the application of the HF-SCF or the B3LYP method in a QMCF-MD simulation. The gas-cluster values for both of these methods show insignificant differences compared to the results of the correlated ab initio CCSD calculations. The Hartree−Fock method was preferred over B3LYP, because the semiempirical B3LYP approach[42] is known to fail for a proper description of H bonds,[24] leading to a too-rigid hydration structure. Generally, in a strongly polarized system like the four-times positively charged uranium(IV) ion in water, energy contributions resulting from electron correlation effects are very small compared to electrostatic energy contributions. Former QMCF-MD simulations of ions in aqueous solution[16−21] gave excellent results at manageable computational effort employing HF-level calculations with double-ζ basis sets. Table 1 also displays the results for average binding energies per ligand employing the Stuttgart RSC 1997 ECP basis set. All energies are identical within a methodological accuracy of ±0.5 kcal/mol.

(25) Mulliken, R. S. *J. Chem. Phys.* **1955**, *97*, 1833.
(26) Dunning, T. H. *J. Chem. Phys.* **1970**, *53*, 6026.
(27) Magnusson, E.; Schaefer, H. *J. Chem. Phys.* **1985**, *83*, 5721.
(28) Rode, B. M.; Schwenk, C.; Hofer, T.; Randolf, B. *Coord. Chem. Rev.* **2005**, *249*, 2993.
(29) Rode, B. M.; Schwenk, C.; Tongraar, A. *J. Mol. Liq.* **2004**, *110*, 105.
(30) Feller, D. *J. Comput. Chem.* **1996**, *17*, 1571.
(31) Schuchardt, K. L.; Didier, B. T.; Elsethagen, T.; Sun, L.; Gurumoorthi, V.; Chase, J.; Li, J.; Windus, T. L. *J. Chem. Inf. Model.* **2007**, *47*, 1045.
(32) Frisch, M. J. et al. *Gaussian 03*, revision C.9.; Gaussian, Inc.: Wallingford, CT, 2004.
(33) Ahlrichs, R.; Bär, M.; Häser, M.; Horn, H.; Kömel, C. *Chem. Phys. Lett.* **1989**, *162*, 165.
(34) Brode, S.; Horn, H.; Ehrig, M.; Moldrup, D.; Rice, J. E.; Ahlrichs, R. J. *Comp. chem.* **1993**, *14*, 1142.
(35) Ahlrichs, R.; von Arnim M. In *Methods and Techniques in Computational Chemistry: METECC-95*; Clementi, E., Corongiu, G., Eds.; STEF: Cagliari, Italy, 1995; Chapter 13, pp 509−554.
(36) von Arnim, M.; Ahlrichs, R. *J. Comput. Chem.* **1998**, *19*, 1746.
(37) Frick, R. J.; Hofer, T. S.; Pribil, A. B.; Randolf, B. R.; Rode, B. M. 2008, Manuscript submitted.
(38) Küchle, W.; Dolg, M.; Stoll, H.; Preuss, H. *J. Chem. Phys.* **1994**, *100*, 7535.
(39) Frick, R. J.; Hofer, T. S.; Pribil, A. B.; Randolf, B. R.; Rode, B. M. 2008, Manuscript submitted.
(40) Ermler, W. C.; Ross, R. B.; Christiansen, P. A. *J. Quant. Chem.* **1991**, *40*, 829.
(41) Ortiz, J. V.; Hay, P. J.; Martin, R. L. *J. Am. Chem. Soc.* **1992**, *114*, 2736.
(42) Becke, A. D. *J. Chem. Phys.* **1993**, *98*, 5648.

The simulation box was a cube of 24.8 Å side length containing one U^{4+} ion and 499 water molecules. The density of 0.997 g/cm^3 corresponds to the density of pure water at 298 K. Periodic boundary conditions were applied and long-range Coulombic interactions taken into account by the reaction field method.[43] The core zone had a radius of 2.5 Å around the central uranium(IV) ion; the entire QM region extended to a sphere of radius 5.7 Å, containing an average of 29 water molecules and, thus, corresponding to two full layers of hydration. The smoothing zone stretches from a distance of 5.5 to 5.7 Å. Temperature control by the Berendsen algorithm[44] was applied to sample a canonical NVT ensemble by coupling the system to a heat reservoir with a temperature of 298.15 K, the coupling constant τ being 0.1 ps. A second-order predictor−corrector integrator of the Adams−Bashforth family was used to integrate the time step, chosen to be small enough to be able to observe explicit hydrogen movements, namely, 0.2 fs. The initial geometry was taken from a simulation box of a former QM/MM simulation of the Mg^{2+} ion.[45] Since the octahedrally coordinated, comparably small and lower charged magnesium(II) ion is a rather rough estimation of the geometry of the hydrated uranium(IV) ion, a long equilibration time (6 ps) was deemed necessary. After only 2 ps of equilibration, the first hydration shell expanded to a then constant volume of nine ligands. A total of 10 ps of sampling was used for determination of the presented data. The simulation took overall 13 months on six Opteron 64-bit processors.

For evaluation of the structure, besides the well-established evaluation tools, conventional three-body distribution functions as well as the newly formulated local density corrected three-body distribution functions $f_{O-X-O}^{(3)}(s,r,s)$[46] were used. Three-particle distribution functions $g_n^{(3)}(r_1,r_2,r_3)(r_1,r_2,r_3)$, in contrast to pair distribution functions, account for the probability of encountering triples of different side lengths.[47,48] For a homogeneous system, they simply can be obtained by counting triples of particles with respective side distances r, s, and t from each other that lie between $r - \Delta r/2 < r < r + \Delta r/2$, $s - \Delta s/2 < s < s + \Delta s/2$, and $t - \Delta t/2 < t < t + \Delta t/2$ and dividing this sum $\bar{n}(r,s,t)$ by the volume element ΔV in which these particles can theoretically be located at given values of Δr, Δs, and Δt.

$$g_n^{(3)}(r_1, r_2, r_3) = \frac{\bar{n}(r, s, t)}{\Delta V} \tag{10}$$

For a species X in aqueous solution, the three-particle distribution function $g_{O-X-O}^{(3)}(r,r,r)$, which gives information about the existence of equilateral triangles, was obtained using

$$g_{O-X-O}^{(3)}(r, r, r) = \frac{\bar{n}(r, r, r)\, V^2 r^3 \Delta r^3}{8\pi^2 N_X N_{OW}(N_{OW} - 1)} \tag{11}$$

To obtain information about the solvent structure in a given solvation shell with respect to the solute X, a modified function $f_{O-X-O}^{(3)}(s,r,s)$, where s is the distance from the solute to the solvent oxygen, was developed, which accounts for the actual local density in a shell of width Δs:[46]

$$f_{O-X-O}^{(3)}(s, r, s) = \frac{\bar{n}(s, r, s)}{8\pi^2 N_X \rho_{shell}^2 r s^2 \Delta s^2 \Delta r} \tag{12}$$

$$\rho_{shell} = \sqrt{\frac{N_{shell}(N_{shell} - 1)}{V_{shell}^2}} \tag{13}$$

The shape of the local density corrected three-particle distribution function $f_{O-X-O}^{(3)}(s,r,s)$ can be compared to the oxygen−oxygen radial distribution function (RDF) for the pure solvent to assess if and to what extent the structure of water within a shell visible in the solute−solvent radial distribution function differs from the structure of the pure solvent.

3. Results and Discussion

3.1. Structure. The strongly charged U^{4+} ion is readily coordinated to water and influences the water structure up to considerably large distances. The RDFs for the water oxygen atoms and the water hydrogen atoms are depicted in Figure 2. A very distinct peak for the first-shell water ligands is observed, with a maximum at a uranium−oxygen distance of 2.45 Å. The value lies within 2% of the experimentally determined distances of 2.44 Å (LAXS[4]) and 2.42 Å (EXAFS[6]). These ligands very strictly orient their oxygen atom toward the uranium, since the first-shell peaks in g_{U-O} and g_{U-H} do not overlap. Integration over the RDF leads to a 9-fold coordination in the first hydration shell, which lies well in between the different experimental data: LAXS experiments have indicated 8-fold coordination,[3,5] while EXAFS experiments produced a coordination number of 10 ± 1.[6] Earlier quantum chemical investigations on the relative stabilities of different uranium−water gas-phase cluster structures have also suggested a first-shell coordination number of 9.[49,50]

For determination of the geometry of the first shell, the angular distribution function (ADF) for the oxygen−uranium−oxygen angles (Figure 3) was examined. It has two maxima at angles of about 70° and 135° and an almost zero-reaching minimum around 100°. Angles below 60° and beyond 160° are never encountered throughout the whole simulation.

There are five regular convex polyhedrons that possess nine vertices: the triaugmented triangular prism, the tridiminished icosahedron, the elongated square pyramid (or capped square prism), the gyroelongated square pyramid (or capped square antiprism), and the triangular cupola (Figure 4). All belong to the same family of polyhedrons, the so-called Johnson solids. All five solids were constructed around a center particle, and the angular distribution functions g_{V-C-V} of the angle between two vertices and the center atom were calculated.

The angular distribution function from Figure 3 was superimposed on the angular distribution functions corresponding to each of the five geometrical Johnson solids

(43) Onsager, L. *J. Am. Chem. Soc.* **1936**, *58*, 1486.
(44) Berendsen, H. J. C.; Postma, J. P. M.; vanGusteren, W. F.; DiNola, A.; Haak, J. R. *J. Phys. Chem.* **1984**, *81*, 3684.
(45) Tongraar, A.; Rode, B. M. *Chem. Phys. Lett.* **2005**, *409*, 304.
(46) Bhattacharjee, A.; Hofer, T. S.; Rode, B. M. *Phys. Chem. Chem. Phys.* **2008**, *10*, 6653.
(47) Krumhansl, J. A.; Wang, S.-S. *J. Chem. Phys.* **1971**, *56*, 2034.
(48) Tanaka, M.; Fukui, Y. *Prog. Theor. Phys.* **1975**, *53*, 1547.
(49) Tsushima, S.; Yang, T.; Mochizuki, Y.; Okamoto, Y. *Chem. Phys. Lett.* **2003**, *375*, 204.
(50) Tsushima, S.; Yang, T. *Chem. Phys. Lett.* **2005**, *40*, 68.
(51) Hofer, T. S.; Tran, H. T.; Schwenk, C. F.; Rode, B. M. *J. Comput. Chem.* **2004**, *25*, 211.
(52) Weast, R. C. *Handbook of Chemistry and Physics*, 54th ed.; CRC Press: Boca Raton, FL, 1973.

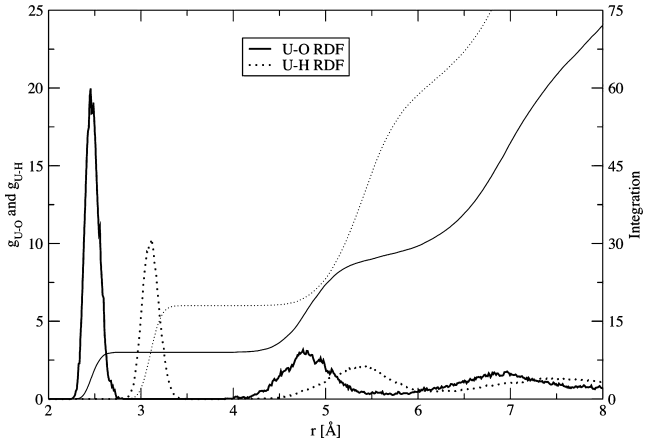

Figure 2. U−O and U−H radial distribution functions and their running integration numbers.

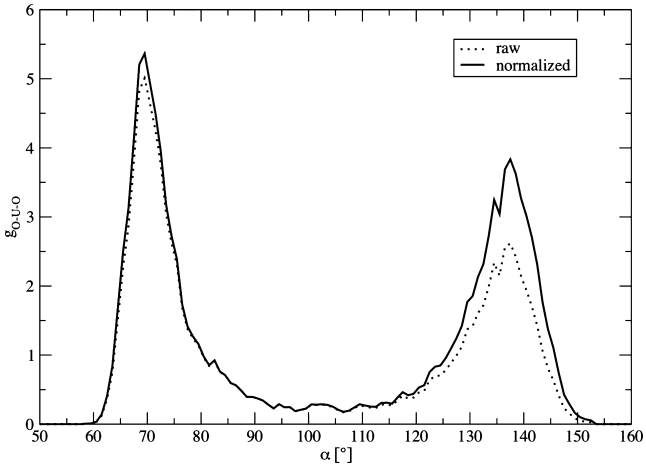

Figure 3. O−U−O angular distribution function.

(Figure 5). The normalized ADF is obtained by applying the following scheme:

$$\mathrm{adf}_{\mathrm{norm}} = \frac{\mathrm{adf}}{\sin(\alpha)}$$

where $\Delta\alpha$ is the bin size for the histogram and adf is the plotted raw data of the angular distribution function.

The g_{O-U-O} of both the ideal tridiminished icosahedron and the ideal capped square prism show an occurrence of angles beyond 160° and would, in a dynamical system, most likely adopt angles below 60°. In the ADF of the triangular cupola, the maxima at angles of 60° and 120° significantly differ from the maxima at angles of 70° and 135° in the function derived from the simulation. The g_{O-U-O} of the ideal triaugmented triangular prism looks similar to the one of our system, but there is a quite large gap spanning over ∼40° in between the maxima. The capped square antiprism (or gyroelongated square pyramid) ADF fits best. The details about the nomenclature and different tricapped trigonal prismatic geometries have been discussed in ref 62. As was stated in that work, among the nine coordinated metal centers, with mono- or bidentate ligands, the preferable structures are r-TCTPR and r-CSAPR. Normally, these five regular convex polyhedrons are also known as "Johnson polyhedra". These polyhedrons, by definition, usually have edges of all the same length. In contrast to that, for coordination compounds, it is important to have center-to-vertex distances that are all equal; under such conditions, the tricapped trigonal prism is abbreviated as r-TCTPR and the capped square antiprism as r-CSAPR. The latter one is also the preferable geometry found for aqueous U^{4+} ion speciation.

The configuration of the first coordination shell of the U^{4+} ion in C_{4v} symmetry corresponding to the idealized geometry of a gyroelongated square pyramid was assumed, therefore, to be the actual configuration. Different screenshots of the visualized trajectory shown in Figure 6 support this assumption, especially the one to the left where all neighboring oxygen atoms are connected and the structure of the gyroelongated square pyramid is recognized, with a single cap in the front sitting on a square and with a square rotated by ∼45° to the front square in the back. The same structure has been proposed for the first hydration shell configuration of U^{4+} in ref 1, too.

By having a closer look at the first oxygen peak in the RDF from Figure 2, the presence of a double peak (2.45 and 2.48 Å) can be detected. This suggests that the nine water molecules in the first layer of solvation may not all be completely equivalent throughout the simulation, which is not contradictory to the assumed first-shell geometry, since in a gyroelongated square pyramid the vertices belonging to the pyramid basis lie slightly closer to the center. The shoulder at 2.7 Å can be explained by partly contributing Johnson-body CSAPR structures which include one water ligand at a longer distance (top of the pyramid, Figure 4e).

The structural data obtained by the QMCF-MD simulation for U^{4+} fit well into a series of highly charged actinoid ions reported in the literature.[11,58−60] A series of actionoid data based on EXAFS and XAFS[58−60] studies is given in Table 2 for comparison.

The g_{U-O} function also indicates the presence of a well-defined second hydration layer with its maximum at a distance of 4.80 Å from the ion and even a third hydration layer at a 6.80 Å distance. The coordination number distributions for the first, second, and third shell (the outer cutoff distance for the second shell was chosen as 5.75 Å; the third shell cutoff was set 8.0Å) are depicted in Figure 7.

(53) D'Incal, A.; Hofer, T. S.; Randolf, B. R.; Rode, B. M. *Phys. Chem. Chem. Phys.* **2006**, *8*, 2841.
(54) Hofer, T. S.; Randolf, B. R.; Rode, B. M. *Chem. Phys. Phys. Chem.* **2005**, *7*, 1382.
(55) Hofer, T. S.; Randolf, B. R.; Rode, B. M. *Chem. Phys. Lett.* **2006**, *422*, 492.
(56) Fakas, I.; Grenthe, I. *J. Phys. Chem. A* **2000**, *104*, 1201.
(57) Fakas, I.; Banyai, I.; Szabo, Z.; Wahlgren, U.; Grenthe, I. *Inorg. Chem.* **2000**, *39*, 799.
(58) Allen, P. G.; Bucher, J. J.; Shuh, D. K.; Edelstein, N. M.; Reich, T. *Inorg. Chem.* **1997**, *36*, 4676.
(59) Allen, P. G.; Bucher, J. J.; Shuh, D. K.; Edelstein, N. M.; Craig, I. *Inorg. Chem.* **2000**, *39*, 595.
(60) Moll, H.; Denecke, M. A.; Jalilehvand, F.; Sandstrom, M.; Grenthe, I. *Inorg. Chem.* **1999**, *38*, 1795.
(61) Küchle, W.; Dolg, M.; Stoll, H.; Preuss, H. *J. Chem. Phys.* **1994**, *100*, 7535.
(62) Ruiz-Martinez, A.; Casanova, D.; Alvarez, S. *Chem.—Eur. J.* **2008**, *14*, 1291.
(63) Batista, E. R.; Martin, R. L.; Hay, P. J. *J. Chem. Phys.* **2004**, *121*, 11104.

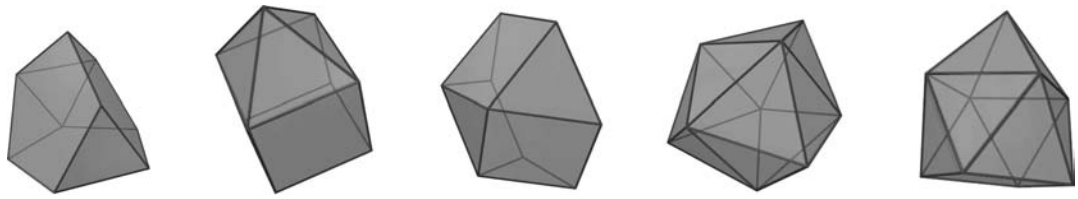

Figure 4. Pictures of five regular convex polyhedrons (Johnson solids) carrying nine vertices. From left to right: (a) a tridiminished icosahedron, (b) an elongated square pyramid, (c) a triangular cupola, (d) a triaugmented triangular prism, and (e) a gyroelongated square pyramid.

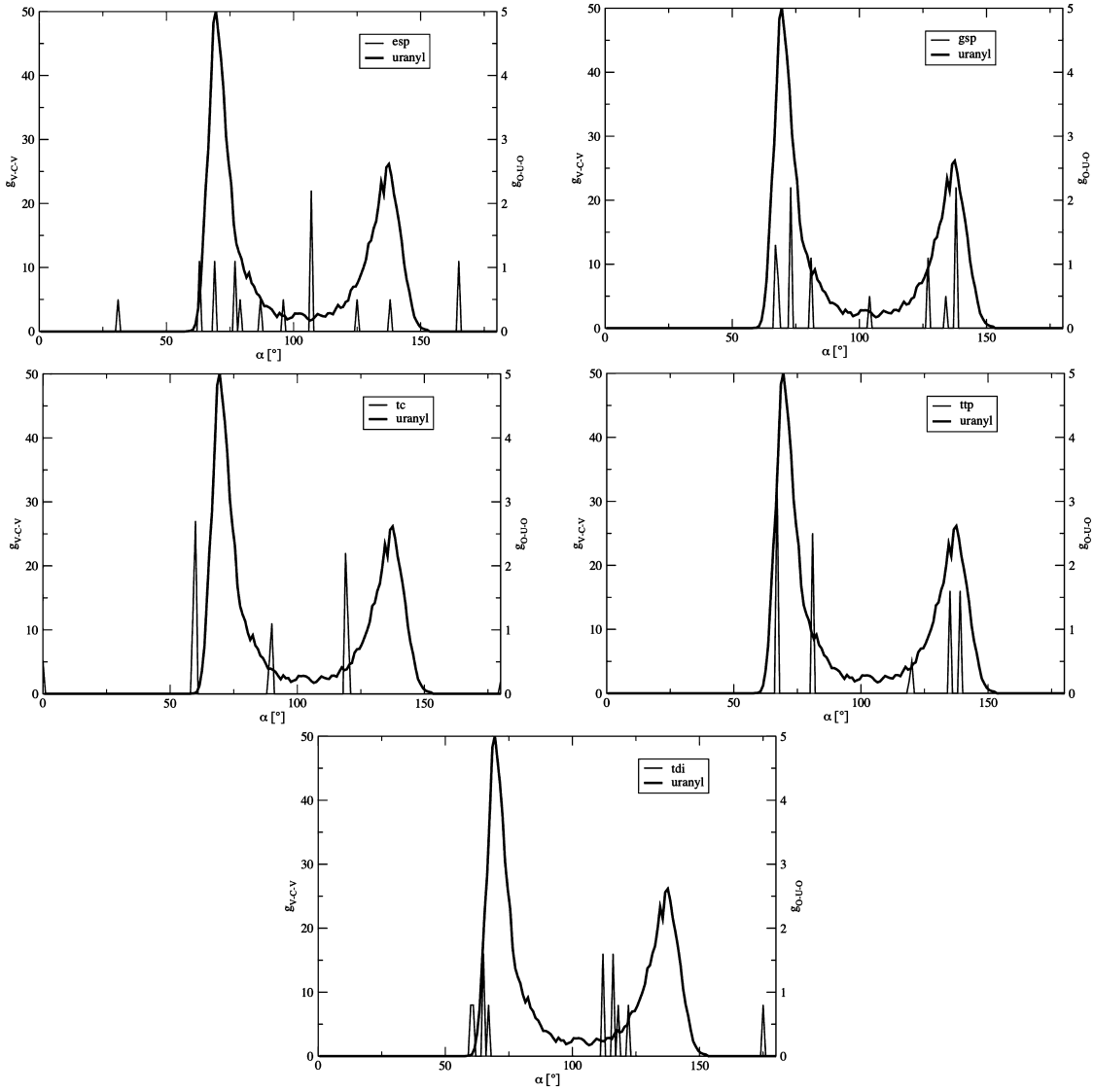

Figure 5. O−U−O angular distribution function (uranyl, bold black) superimposed on the V−C−V angular distribution functions for an elongated square pyramid (esp), a gyroelongated square pyramid (gsp), a triangular cupola (tc), a tricapped triangular prism (ttp), and a tridiminished icosahedron (tdi).

It shows that 19 is the preferred coordination number in the second shell, other encountered coordination numbers ranging from 17 to 21, and that the third shell contains between 37 and 49 water molecules, peaking at 44.

The tilt- and Θ-angle distributions calculated for the first shell (Figure 8) show the orientation of the coordinating water molecules. The tilt angle is the angle between the solute−ligand oxygen vector and the plane spanned by the three atoms of the water, the Θ angle is the angle between the solute−ligand oxygen vector and the resulting vector from the addition of the two hydrogen−oxygen vectors within one water molecule. The sharp maxima at 0° for the tilt angle and at 180° for the Θ angle indicate that throughout the whole simulation time the dipole vectors of the coordinating water molecules do not drift from pointing toward the ion by more than 30°. This is in agreement with the absence of any overlap between the uranium−oxygen and the uranium−hydrogen radial distribution functions with respect to sampling time, an indication of a highly stable first shell common for multiply charged cations. An overview of the structural data obtained in comparison to experimental data is given in Table 3. Very good agreement with the experiment is achieved as far as the distance of the uranium ion to the first hydration shell is concerned. Further, the two

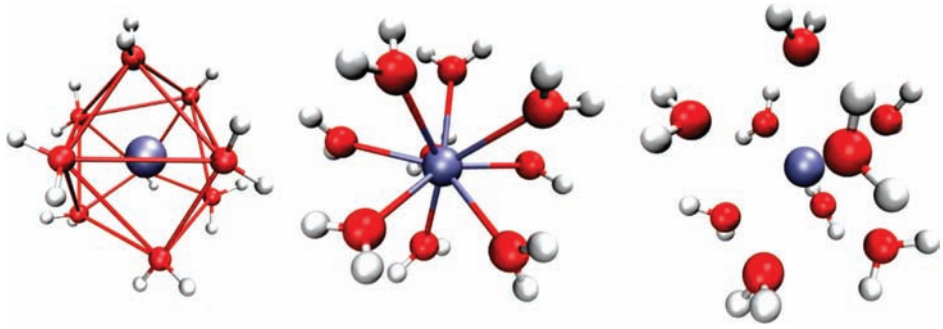

Figure 6. Screenshots from the U^{4+} simulation trajectory. The left picture connects all oxygen atoms of neighboring water ligands; the middle screenshot shows bonds from uranium to the coordinating oxygen atoms. A plain screenshot is given on the right-hand side.

Table 2. Data for the Hydration Structure of Actinoid Ions and Our QMCF-MD Simulation

	method	ion−O distance	CN first shell
Th^{4+} 1.5 M $HClO_4$[60]	EXAFS	2.45	10.8 ± 0.5
U^{4+} 1.5 M $HClO_4$[60]	EXAFS	2.42	10.8 ± 0.5
U^{4+} QMCF-MD	QMCF-MD	2.45	9.0
Np^{4+} 1 M HCl[58]	XAFS	2.40	11.2
Pu^{3+} 0.01 M LiCl[58]	XAFS	2.51	10.2
Am^{3+} 0.25 M HCl[59]	EXAFS	2.48	10.3
Cm^{3+} 0.25 M HCl[59]	EXAFS	2.45	10.2
Cm^{3+} 0.25 M HCl[11]	DFT/MD	2.47−2.48	9

different experiments deliver coordination numbers for the first shell that deviate significantly, by about 2.5 ligands, from each other. The value of 9 from the QMCF-MD simulation lies well between these two different coordination numbers from LAXS[4] and EXAFS[6] experiments.

Table 3. Data for the Structure of the Hydrated U^{4+} Ion Obtained from the QMCF Simulation and Experiments

	QMCF-MD	LAXS	EXAFS
U−O distance first shell	2.45 Å	2.44 Å[4]	2.42 Å[6]
U−O distance second shell	4.80 Å		
U−O distance third shell	6.80 Å		
CN first shell	9	8.2 ± 0.4[4]	10.8 ± 0.5[6]
CN second shell	19 ± 2		
CN third shell	44 (37 to 49)		

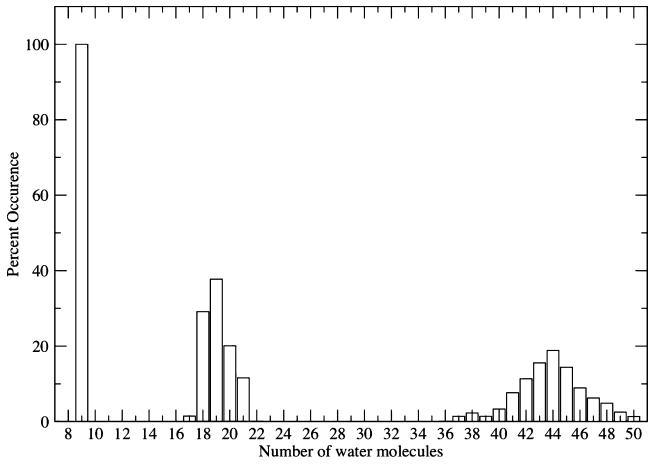

Figure 7. Coordination number distributions for the first, second, and the third shell of the hydrated uranyl(IV) ion.

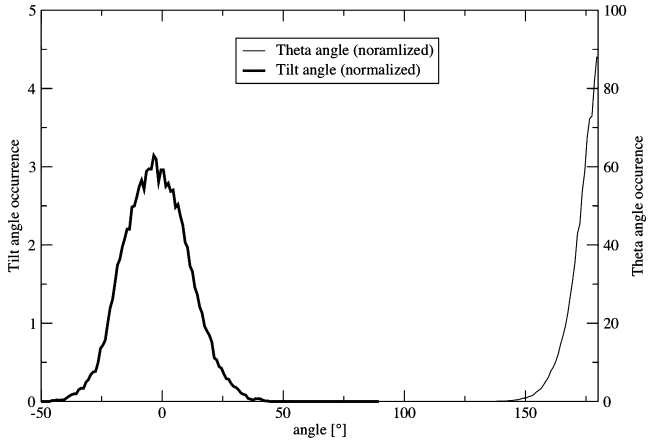

Figure 8. Tilt- and Θ-angle distribution for the first shell.

Local density corrected three-body distribution functions $f_{O-X-O}^{(3)}(s,r,s)$ were plotted for the first-shell oxygen atoms up to a distance of 2.8 Å and for the second-shell oxygen atoms ranging from 4.25 to 5.5 Å and compared to the oxygen−oxygen pair distribution function for pure water obtained from a QM/MM simulation of pure water[24] (Figure 9). The usage of local density corrected three-body distribution function $f_{X-O-O}^{(3)}(s,r,s)$ for U−O−O is to describe the quantitative and qualitative solvent structure reorganization by the presence of a solute in a region at a given distance range. The existing solvent structure is primarily described by an O−O radial distribution function. In a region of no influence by the solute, this particular function is supposed to coincide with the pure solvent radial pair distribution function. Obviously, the first hydration shell strongly differs from the pure solvent, and the gyroelongated square-pyramidal structure is well-reflected. The second shell also displays a structure definitely different from bulk solvent.

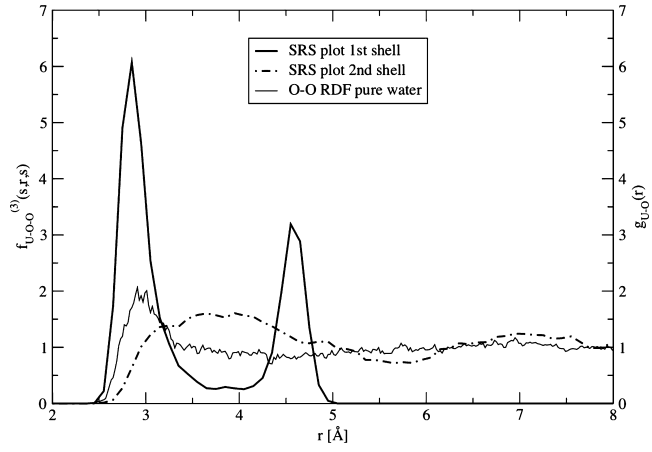

Figure 9. Local density corrected uranium−oxygen−oxygen three-body distribution functions for the first and second shells of hydration. Overlay to the oxygen−oxygen pair distribution function for the pure solvent[24] is given for comparison.

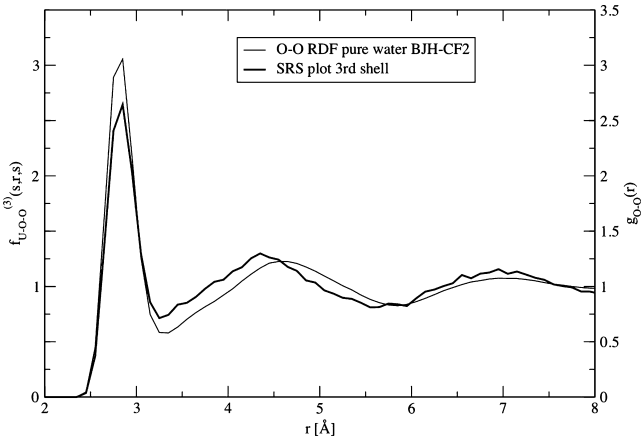

Figure 10. Local density corrected uranium−oxygen−oxygen three-particle distribution function for the third shell of hydration. An overlay with the oxygen−oxygen pair distribution function for the BHJ-CF2 water model.[22,23]

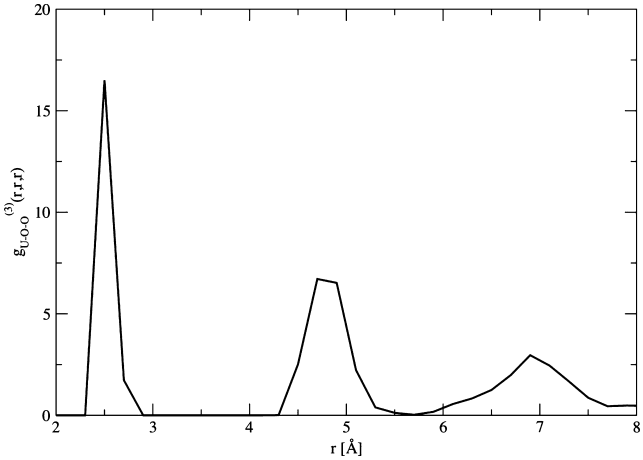

Figure 11. The oxygen−uranium−oxygen triple distribution function for U^{4+} in water.

To emphasize the geometrical and electronic distortion of the first-shell water molecules, distances and angles were evaluated for the first hydration layer and the bulk solvent molecules. The average HOH angle is 107.1° in the solvent molecules close to the uranium ion, compared to 101.5° in the bulk. Another significant geometrical change of +4−5% is found in the OH distance for all nine water molecules in the first shell.

The same function $f_{X-O-O}^{(3)}(s,r,s)$ also was established for the third shell and superimposed on the O−O RDF obtained by a classical molecular mechanics simulation for pure water corresponding to the classical BHJ-CF2 model (Figure 10),[22,23] because the third layer of solvation already lies outside the QM region. As expected, the similarity of the two functions is closer than for the two inner hydration layers, but the second maximum is shifted to lower values of r, indicating that a weak third layer of hydration is formed.

A conventional three-body distribution function, $g_{O-X-O}^{(3)}(r,r,r)$, was also plotted and is shown in Figure 11. This is interesting because the uranium(IV) ion shows a very distinct peak for its first shell due to its first-shell geometry. This is only possible if equilateral triangles of U−O−O are formed and reflects the occurrence of angles around 60° in the angular distribution function for the first shell (Figure 3), within some tolerance resulting from Δr used to obtain $g_{O-X-O}^{(3)}(r,r,r)$. This contrasts with the same plots for ions showing tetrahedral or octahedral coordination, where angles in the ADF of around 60° are absent. Among those, only ions with a flexible first shell can be expected to show a peak like this, but never that distinct.

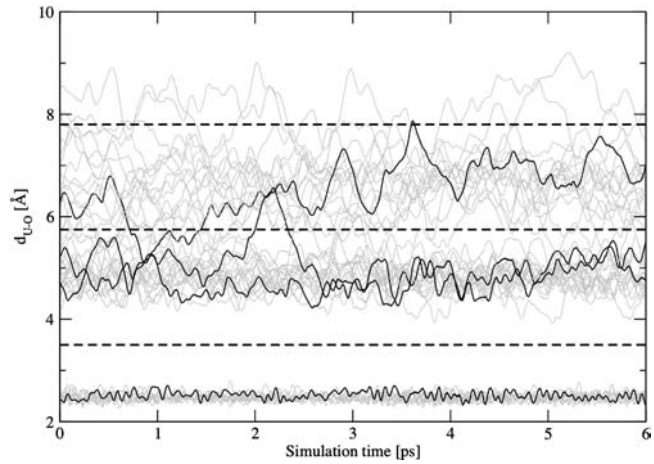

Figure 12. Plot of distances between uranium and the first- and second-shell water oxygen atoms.

Table 4. Characteristic Data for the Solvent Dynamics for U^{4+}, Other Aqueous Ions, and Pure Water

	CN_{first}	q/r_{ion} [e/Å]	q/r_{hydr} [e/Å]	$N_{ex}^{0.5}$/ 10 ps	$N_{ex}^{0.0}$/ 10 ps	$\tau_{0.5}$ [ps]	$\tau_{0.0}$ [ps]	$1/S_{ex}$
U^{4+}	9	4.1	1.2					
second shell				23	136	8.1	1.4	5.9
third shell				61	716	4.6	0.6	11.7
Al^{3+} [54,55]	6	5.9	1.0					
second shell				4.7	68	26.4	1.8	15
Be^{2+} [53]	4	5.7	0.8					
second shell				22	223	4.8	0.4	10.0
third shell				86	1120	3.2	0.3	13.0
H_2O [24]	4			24	268	1.7	0.2	11.2
U^{4+} [56]	10 ± 1	4.1	1.2					
first shell						1.9×10^5		
Th^{4+} [56]	10 ± 1							
first shell						$>0.2 \times 10^5$		

3.2. Dynamics. Values for g_{U-O} (and g_{U-H}) equal zero between the first and second peak (Figure 2), attesting to the absence of any water exchange reactions during the whole sampling time. The nonzero minima between the second and third shell, and between the third shell and bulk water, suggest water exchange between the second and third shell and the third shell with the bulk. A distance plot of the U−O distances between the ion and all water ligands that ever stayed in the first or second shell (outer cutoff distance was 5.75 Å) is given in Figure 12.

While the vibrations of the first-shell water molecules are restricted to a very small amplitude and no exchanges occur, multiple exchange processes are observed in the second and third shells. Some representative movements of individual water molecules are highlighted: a water molecule residing in the first shell, a water molecule remaining in the second shell, a water molecule exchanging from the second shell into the third one, and a water molecule exchanging from the third to the second shell.

In Table 4, mean residence times and related data are summarized and compared to values for other strongly

polarizing ions as well as pure water. The mean ligand residence times τ in picoseconds were evaluated by the direct method.[51] Further characteristic data listed are the number of observed ligand exchange events per 10 ps simulation time, N_{ex}, persisting for $t^* = 0.0$ and 0.5 ps and the reciprocal of the sustainability coefficient $S_{ex} = N_{ex}^{0.5}/N_{ex}^{0.0}$ corresponding to the number of migration attempts needed to achieve one sustainable exchange event. Additionally, coordination numbers of the ion's first shell and the charge per ionic radius for the isolated ion, q/r_{ion}, and for the ion and its first solvation shell (cutoff distance was the outer end of the first-shell hydrogen peak in the corresponding RDFs), q/r_{hydr}, are given. Values for the radii of the isolated ions (U^{4+}, 0.97 Å; Al^{3+}, 0.51 Å; Be^{2+}, 0.35 Å) were acquired from ref 52, for the hydrated ions (U^{4+}, 3.4 Å; Al^{3+}, 3.0 Å; Be^{2+}, 2.6 Å) apart from the U(IV) from two-shell QM/MM approaches.[53,54]

The mean residence times allow an interesting comparison with some other ions in water, especially Be(II)[53] and Al(III).[54,55] These two ions form a third hydration shell just like U(IV), but their adequacy for comparison is better understood considering the similar values of ionic charge per radius given in Table 4. The large ionic radius together with the bulky first coordination shell holding nine ligands effect that, although the uranium(IV) ion possesses the highest formal charge, its charge density at the surface is not higher than the charge density of the other ions mentioned, and thus mean residence times cannot be expected to be particularly high. The mean residence time in the second shell of the aqueous Al(III) ion even considerably exceeds that of U(IV), which can be attributed to stronger hydrogen-bond formation between the first and second shells in the case of Al^{3+}. This in turn may be caused by more strongly polarized first-shell ligands in the aluminum hydrate. Still, mean ligand residence times $\tau_{0.5}$ of the U^{4+} ion in water were determined as 8.1 ps for a ligand in the second and 4.6 ps for a ligand in the third shell, counting only those exchange events lasting more than 0.5 ps, a time which is considered most appropriate since it corresponds to the average lifetime of a hydrogen bond in water.[51] Both the second- and the third-shell values for the mean residence time exceed the value for pure water, thus attesting to the U^{4+} ion structure-forming activity up to the third shell. The mean residence times are higher than those for the small Be(II) ion because this system has a considerably lower charge density outside its first hydration shell. Experimental values for the exchange of first-shell water ligands are given for the ions uranium and thorium[56] too, clearly indicating that mean residence times are orders of magnitude longer than any feasible time for the QMCF method.

The screenshot shown in Figure 13 illustrates some hydrogen bonds typical for the solvent molecules in the first two hydration shells of the ion. The first-shell ligands most of the time form two stable hydrogen bonds to the ligands of the second shell (hydrogen bonds numbered 1 and 2 in Figure 13), which accounts for the stability of the second shell despite the size of the first shell. The effective charge of the uranium(IV) ion in aqueous solution was monitored over the whole simulation, and its development over a

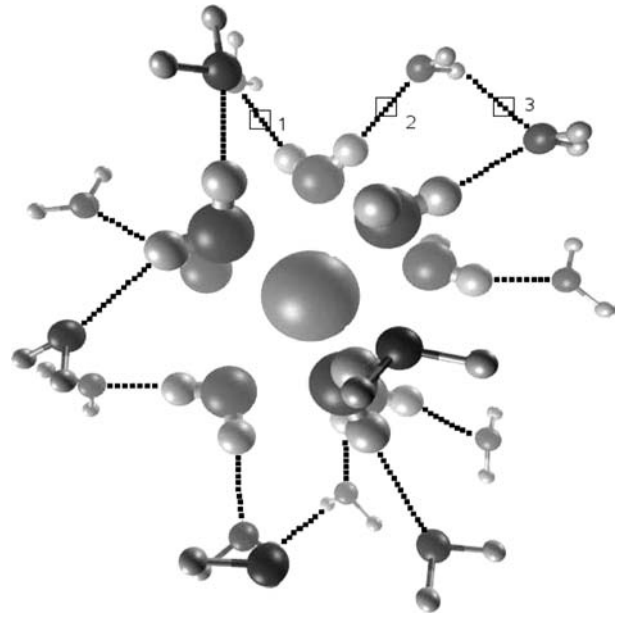

Figure 13. Screenshot of the uranium(IV) ion, its first and selected parts of its second hydration shell. The dotted lines illustrate hydrogen bonds.

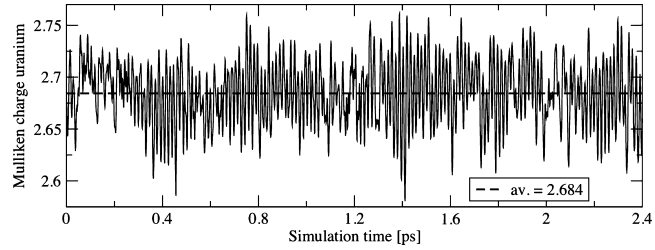

Figure 14. Development of the effective uranium charge over a selected span of time.

representative time frame is given in Figure 14. The average was determined at +2.68 (ranging from +2.58 to +2.76) by Mulliken population analysis;[25] hence, the surrounding water molecules transfer quite a bit of electron density to the ion. First-shell ligand hydrogen atoms therefore are especially prone to forming stable hydrogen bonds. Second-shell ligands also quite often interconnect through hydrogen bonding (hydrogen bond number 3 in Figure 13). First-shell ligands hardly show such behavior.

The considerable charge fluctuation of ±0.2 in Figure 14 also underlines why the preference of the QMCF-MD method over conventional QM/MM approaches is crucial for a successful treatment of this system, since charges are updated in every step of the simulation according to the actual partial charges of the QM particles. Working with constant values for the point charges presents a considerable source of errors.

4. Conclusion

This paper summarizes the first comprehensive theoretical treatment of the uranium(IV) ion in aqueous solution and yields results for the structure that are in excellent agreement with experimentally determined data.[3−6] Coordination numbers of 9, 19, and 44 water molecules have been found for the first, second, and third shells, respectively. The simulation results should prove valuable for the interpretation of future experimental measurements and prove the possibility of

obtaining excellent results for actinides using the QMCF-MD method. The stable high charge of the U^{4+} ion in water induces a very interesting solvent coordination, serving as a good example for the usefulness of analysis tools like the local density corrected three-particle distribution function.[46]

The QMCF-MD framework[14] proved once more its accuracy and additionally its applicability to (in terms of electron numbers) very large solutes. As the computational power available increases, it constitutes a very promising tool for accessing microscopic properties of increasingly complex species in aqueous solution.

Acknowledgment. Financial support for this work from the Austrian Science Foundation (FWF) is gratefully acknowledged.

IC801554P